Robotica (2019) volume 37, pp. 656–674. © Cambridge University Press 2018
doi:10.1017/S0263574718001248

A Systematic Design Selection Methodology for System-Optimal Compliant Actuation

Abdullah Kamadan*, Gullu Kiziltas, and Volkan Patoglu

Faculty of Engineering and Natural Sciences, Sabanci University, Istanbul, Turkey
E-mails: gkiziltas@sabanciuniv.edu; vpatoglu@sabanciuniv.edu

(Accepted October 27, 2018. First published online: November 29, 2018)

SUMMARY
This work presents a *systematic* design selection methodology that utilizes a co-design strategy for system-level optimization of compliantly actuated robots that are known for their advantages over robotic systems driven by rigid actuators. The introduced methodology facilitates a decision-making strategy that is instrumental in making selections among system-optimal robot designs actuated by various degrees of variable or fixed compliance. While the simultaneous co-design method that is utilized throughout guarantees systems performing at their full potential, a homotopy technique is used to maintain integrity via generation of a continuum of robot designs actuated with varying degrees of variable and fixed compliance. Fairness of the selection methodology is ensured via utilization of common underlying (variable) compliant actuation principle and dynamical task requirements throughout the generated system designs. The direct consequence of the developed methodology is that it allows robot designers make informed selections among a variety of systems which are guaranteed to perform at their best. Applicability of the introduced methodology has been validated using a case study for system-optimal design of an active knee prosthesis that is driven by a mechanically adjustable compliance and controllable equilibrium position actuator (MACCEPA) under a periodic/real-life dynamical task.

KEYWORDS: Co-design methods; Variable stiffness actuators; Optimal control; Optimal design.

1. Introduction

The design philosophy behind industrial robots is mainly centralized around the objectives of high repeatability and accuracy, making them heavy and rigid systems that are energetically inefficient and unsafe to interact with. On the contrary, inspired by their biological counterparts, design of robots powered with compliant actuators is aimed at emulating the working principles of biological systems which are highly sophisticated machines with regard to areas in energy efficiency, safety, and performance. Through the use of typically antagonistically arranged muscles around their joints, biological systems are able to regulate their compliance independent of joint position. This enables them to use potential energy stored in their joints in making them very efficient during repetitive tasks such as running, hopping, and walking. Compliance regulation also makes them perform better at tasks such as throwing, hammering, kicking, at the same time making them very adaptive for safe interaction with their environments.

Motivated by these advantages, considerable work has been expended by researchers in the field of robotics to take advantage of compliant actuation in various ways. One of the most notable examples regarding compliance in robot actuation has been the series elastic actuation (SEA). SEAs were introduced and analyzed to show significant advantages over conventional rigid actuation for natural

* Corresponding author. E-mail: kamadan@sabanciuniv.edu

tasks with regard to areas in force control, interaction safety and energy efficiency.[1] After their introduction, SEAs have been developed and employed for numerous robotic applications including prosthetics,[2,3] energy-efficient orthoses,[4] and force-controlled micro-manipulation.[5] SEAs have additionally been demonstrated to provide performance improvements over rigid actuators in tasks, such as speed improvement[6,7] and work output amplification.[8]

Physical compliance of an SEA is determined by the passive spring element that is employed and therefore can only be changed off-line. On the other hand, variable stiffness actuators (VSAs) can physically modulate their compliance during task execution. Active regulation of passive compliance enables VSAs to be employed for designing robots that can approach safety, efficiency, and performance levels found in humans and other biological systems. Over the recent years, various designs of VSAs have been developed in order to exploit the benefits of compliance controllability in robots. Some of the significant VSA designs include the biologically inspired compliant joint,[9] the VSA,[10] bidirectional antagonistic variable stiffness joint,[11] mechanically adjustable compliance and controllable equilibrium position actuator (MACCEPA),[12] actuator with adjustable stiffness,[13] and variable negative stiffness actuator.[14]

In addition to the research work focusing on designing VSA mechanisms, a number of attempts to fully utilize performance benefits of existing designs, mostly using optimal control theory, have also been carried out. Most of these works have focused around improvement of performance merits related to interaction safety and task performance. An optimal control scheme to achieve minimum-time point-to-point motion while guaranteeing safety constraints has been implemented in ref. [15]. Optimal storage of potential energy in variable stiffness joints has been explored in refs. [16] and [17], where problem of achieving maximum link velocity at a given position and a final time, respectively, has been addressed through the use of optimal control theory. It has been demonstrated in ref. [16] that using a VSA enables speed improvements of up to 30% over an SEA. In addition, experiments obtained through the proposed optimal control approach in ref. [16] have led to the conclusion that robots driven by variable compliant actuators outperform their rigid counterparts and, therefore, may enable us to approach performance levels found in humans.

It may be observed that most of the research efforts toward maximum utilization of compliant actuation have been focusing around either designing actuation mechanisms or designing controllers for existing actuation mechanisms. Note that robots powered by compliant actuators are mechatronic systems, in particular, *controlled mechanical systems* which consist of a mechanical *subsystem*, or a plant, as well as a control *subsystem*. In consequence, their overall performance depends on the *synergetic* performance interactions between these subsystems. From a system-level design viewpoint, synergetic interactions between the subsystems are called *design couplings*[18] and must be considered in order to come up with designs that perform at their best potential. Strategies that take into account these design couplings and thereby guarantee designs performing at their full potential, in other words, designs that are *system optimal*, are called *co-design* strategies.[19,20] Two co-design methods that guarantee system-level (local) optimality have been recently demonstrated to provide over 50% performance improvements over conventional approaches, such as control optimization alone,[15–17] for the design of robots driven by variable compliant actuators.[19,20] Accordingly, employment of co-design methods is an essential element to consider when designing optimally performing robots driven by (variable) compliant actuators.

Inclusion of (variable) compliance to a design can result in significant enhancements of several metrics, such as torque, or speed output and a more effective system design as demonstrated in literature. In particular, through the inclusion of controlled compliance, the fixed amount of energy required for the task is better distributed in such a way that peak power requirements (i.e., the peak-to-peak difference of the input torques) are minimized.[20] However, performance trade-offs exist, for instance in terms of design complexity or actuator bandwidth. Note that, with respect to a rigid actuator, the design complexity of a (variable) compliant actuator is higher due to the introduction of an additional motor needed to control the compliance and the involvement of elastic elements which also reduce system bandwidth. Studying such trade-offs is a crucial part of the development process for robotic systems powered by (variable) compliant actuators. These trade-offs are especially important while making design decisions regarding the amount of compliance and/or compliance variation that may be desired in a particular application of interest. Provided examples demonstrate significant findings in respect to performance enhancements that can be achieved by employment of

https://doi.org/10.1017/S0263574718001248 Published online by Cambridge University Press

(variable) compliant actuation. In the meantime, a comparative analysis to systematically study the aforementioned trade-offs is still missing.

1.1. Contributions

In ref. [20] the authors presented two alternative co-design optimization methods that guarantee system-optimal designs for controlled mechanical systems and successfully implemented them on system-level design of robots powered by controllable compliant actuators. This paper, on the other hand, uses only one of the co-design methods introduced in ref. [20], namely the simultaneous (SIM) method due to its ease of implementation, as the basic optimizer tool of choice.

In this paper, the authors develop a novel multi-criteria design selection methodology for robots powered by (controllable) compliant actuators for a chosen VSA system. More specifically, given a variable stiffness actuation platform, such as MACCEPA, the proposed methodology provides system-optimal solutions for different design preferences. The design preferences are based on a continuous search implemented through a two-phase design process that allows for a fair comparison. The introduced methodology is novel in that it is *systematic*, utilizes *Pareto*-optimization, and implements a *homotopic* procedure.

More specifically, the work in this paper adds to[20] the following contributions:

(i) develops a *systematic* design comparison methodology that enables engineers make *fair* and *unbiased* design decisions for system-optimal designs of compliantly actuated robots with varying levels of controllable or fixed compliance (FC);
(ii) introduces a *Pareto*-optimization-based design comparison structure where each design is system optimal and enables engineers study trade-offs and make well-informed design preferences; and
(iii) uses a mathematically sound *homotopic* process to establish design continuity and integrity throughout controllable and FC designs and thereby provides a fair comparison architecture among these architectures.

Related to the above three key features of the novel design selection methodology, the following can be emphasized:

The *systematic* design selection methodology proposed in this paper generates system-optimal designs, each performing at its maximum potential for a given application, hence, provides an unbiased design guidance for robots driven by compliant actuation systems. Please note that the introduced approach is *systematic* in the sense that it provides integrity among all of the generated designs, for a given dynamic application. This integrity is ensured by maintaining certain key design aspects throughout generated designs, as listed in Section 2.1. In addition, one of the key features of the proposed methodology is that it provides a design comparison architecture that enables fair and well-informed engineering decisions.

The *Pareto*-based methodology provides a set of Pareto-optimal solutions which is instrumental in allowing engineers to study design trade-offs, such as system complexity and actuator bandwidth. These trade-offs may be involved in adding increased compliance to a robot joint and/or when adding further actuation effort to control the level of compliance at a joint, during the execution of a predetermined task.

The implemented *homotopy* approach is used to deliver a range of successive system-optimal design solutions within a local design neighborhood. Homotopic techniques are numerical continuation methods whose basic principle is to solve a problem by relating it to the known solution of a somewhat easier problem that is linked, through a homotopy, to the problem in question. By continuously deforming the known solution into the other, a homotopy between two functions is generated. In this work, a similar idea is applied for generating a homotopy, in other words a continuum of system-optimal designs with different levels of variable compliance (VC) and/or FC. This way, overall integrity of the design selection methodology is guaranteed.

To the best of authors' knowledge, a comparison methodology with above key three features does not exist for (controllable) compliant actuation mechanisms. Moreover, in addition to its theoretical importance, the presented work provides a significant contribution in terms of its practical applicability for guiding engineers in selecting among a set of controllable and fixed compliant or rigid actuation designs for their applications.

https://doi.org/10.1017/S0263574718001248 Published online by Cambridge University Press

On a final note, although the presented work is related to stiffness/compliance modeling of VSA systems and multi-objective optimization, the main focus of the paper is about using system-level optimization techniques to analyze VSAs. In the meantime, three review papers are included in references on the subjects to refer the readers who may be interested in compliance modeling and multi-objective optimization.[21–23]

1.2. Structure

The paper is organized as follows: Section 2 presents the preconditions for an unbiased comparison of designs, introduces the system-optimal co-design method used throughout the selection problem, and provides a formal definition for the proposed systematic design selection methodology. Section 3 then demonstrates application of the proposed design selection methodology through a case study. Results for the case study along with implementation details related to the selection methodology are provided in Section 4, while these results are thoroughly discussed in Section 5. The paper is concluded with Section 6, which also presents future research directions.

2. Problem Formulation for the Systematic Design Selection Methodology

This section presents the fundamental constituents of the systematic design selection methodology proposed in this work. Necessary components of the proposed methodology for establishing fairness and integrity among (variable) compliance system designs are listed. This is followed by details related to each one of these components.

2.1. Comparative evaluation of designs with varying (variable) compliance

Performance comparison among robot designs actuated by varying degrees of (variable) compliance is a nontrivial task. This is mainly due to the challenge in performance evaluation of each design in a fair and integrated manner. A systematic design selection methodology that provides fair comparability of such designs needs to include the following main components:

(i) Each design needs to be evaluated and compared at its maximum performance potential for fairness of the analysis. This condition can only be guaranteed by ensuring system-level optimality of every design solution. In other words, each design configuration should feature optimal mechanisms along with corresponding optimal controllers so that every compared design utilizes its maximum capacity.

(ii) To ensure continuity among compared design solutions, every design that is generated during system-level optimizations should be related to each other through a homotopic process. The homotopic process generates results that are valid within the same design neighborhood for the optimization problem that relies on local solvers where all optimal designs are initialized from another neighboring optimal design.

(iii) All of the designs need to be based on a uniform underlying (VC) actuation principle to reinforce the overall integrity of the methodology.

(iv) A common set of dynamical task requirements along with a common system-level design objective should be used in system-level optimization of every design solution.

2.2. Co-design approaches for system-optimal designs

As already pointed out in Section 2.1, a fair selection among system designs is possible only if all of the compared designs perform at their maximum potential. Therefore, an unbiased selection methodology necessitates employment of co-design approaches which guarantee optimally performing controlled mechanical systems. A co-design method optimizes both the mechanical subsystem with respect to static design variables and constraints, along with the control subsystem with respect to dynamic design variables and constraints, for a given system-level design objective in an all at once fashion. Two co-design approaches that guarantee system-level optimality of designs are the SIM and the nested methods. Depending on a particular design application of interest, both methods have their specific advantages and disadvantages that may prompt the use of one method over the other. An in-depth comparison analysis and discussion on each co-design method can be found in ref. [20].

Although both co-design methods are perfectly adequate approaches in coming up with system-optimal designs of robots driven by compliant actuators, the SIM approach has been selected as the preferred method of choice for the proposed design selection methodology. This is due to its advantages in terms of implementation simplicity and convergence speed for this particular problem. The

https://doi.org/10.1017/S0263574718001248 Published online by Cambridge University Press

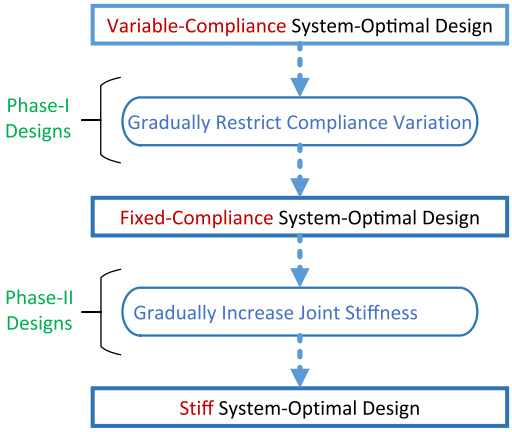

Fig. 1. Homotopy-based design methodology.

SIM approach concurrently treats all of the static/mechanical and dynamic/control design variables along with their respective constraints in the context of a single optimization problem. Mathematical definition of a co-design problem using the SIM strategy can be given as follows:

$$\min_{d_m, d_c} J(d_m, d_c), \quad \text{subject to} \tag{1}$$
$$g_m(d_m, d_c) \le 0, \quad h_m(d_m, d_c) = 0, \quad l_m \le d_m \le u_m$$
$$g_c(d_m, d_c) \le 0, \quad h_c(d_m, d_c) = 0, \quad l_c \le d_c \le u_c$$

Here, J is the system-level cost function (design objective) to be minimized with respect to mechanical and control design variables, d_m and d_c. The mechanical design variables are static (with respect to their respective body reference frames) variables, such as link lengths, link inertias, and spring coefficients, while the control design variables are time varying trajectories which themselves are functions of time. An example trajectory can be the input torque trajectory of an actuator employed in the system. Note that co-design optimization problem is defined over the mechanical and the control equality constraints, h_m, h_c, their inequality constraints g_m, g_c, and lower and upper bounds, l_m, u_m, l_c, u_c, on the mechanical and control design variables, respectively.

2.3. Architecture of the design selection methodology

Robotic systems driven by (variable) compliant actuators are, in general, highly nonlinear systems. Moreover, as suggested in the mathematical definition given in Section 2.2, their system-level designs require solution of a hybrid static/dynamic optimization problem that usually has a non-convex design space. State-of-the-art solvers that focus on such optimization problems are commonly based on local search methods and therefore can guarantee local optimality within neighborhood. This makes the results of such optimization problems strongly dependent on an initial design guess. Establishment of a fair design selection methodology therefore requires a systematic approach that maintains continuity among generated system designs by considering their initialization dependency.

As a means of maintaining continuity, and therefore comparability, among system designs with different levels of VC and FC, the homotopic approach which was described earlier in Section 1.1 has been implemented in this work. This way, a continuum of system-optimal designs starting from VC, moving to FC, and ultimately arriving at a stiff (STF) solution is generated.

Figure 1 represents the architecture of this homotopy-based design methodology and illustrates the main steps involved in the formation of system-optimal designs with different degrees of VC or FC.

The figure highlights two main design stages denoted as Phase-I and Phase-II designs. Each one of these phases represents a continuum of system-optimal design solutions generated between VC, FC, and STF designs. In particular, the architecture is initialized from a system-optimal design with full VC that is obtained using the SIM co-design optimization method without any constraints on variation of compliance. Phase-I designs are then generated using this resulting design as the initial guess for the next optimization problem. This design process is iteratively advanced further while gradually restricting constraints on compliance variation of each design at every iteration until a system-optimal

https://doi.org/10.1017/S0263574718001248 Published online by Cambridge University Press

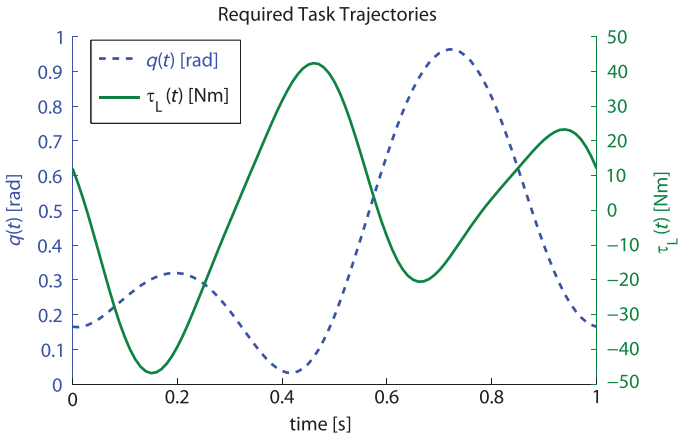

Fig. 2. Dynamic task trajectories.

design with FC is obtained. Similarly, Phase-II designs are iteratively generated using this FC design as the initial guess for the next optimizations while gradually restricting joint compliance at each iteration until an STF system design is reached.

Note that the proposed design methodology ensures a fair comparative analysis by maintaining continuity throughout system-optimal designs in Phase-I and Phase-II homotopy regions.

2.4. Task requirements

In establishing a unified design selection methodology, we have determined a common set of dynamic task requirements which need to be satisfied by each design that gets generated. For the example problem chosen, namely the design of a human knee prosthesis powered by a VSA, these correspond to the following task requirements: the necessary motion $q(t)$ and load torque $\tau_{\mathrm{L}}(t)$ trajectories that need to be maintained at a human knee joint at each period of its gait cycle. For this purpose, periodic trajectories shown in Fig. 2 which were obtained from the human walking data in ref. [24] are used as task specifications. Please note that a single generic optimal VSA design does not exist for all possible dynamic tasks, but it can only be optimal for a particular (given) desired task. That is, the goal is to find the system-level optimal for a given task. Without the specifications of the task, the optimization problem cannot be solved.

As the final required component for a fair design selection methodology, a common system-level design objective has been determined. As our design objective, we have selected to use the dynamic torque range of each actuator used to drive the VSA. The dynamic torque range is defined as the difference between the minimum and the maximum amplitudes of torque trajectories $\tau_1(t)$ and $\tau_2(t)$ that is input from each motor to the system while satisfying the task requirements given in Fig. 2. Note that the selected design objective is a system-level objective. This is because the dynamic torque range of the actuators that is required to be input to the system depends both on the optimally selected design variables of the plant, such as link lengths and inertias and spring coefficient, in addition to the optimally selected design variables of the controller which happen to be the torque trajectories of the motors.

3. CASE STUDY: System-Optimal Design Selection Methodology as Applied for the MACCEPA-Powered Prosthesis

To demonstrate applicability and the effectiveness of the proposed design selection methodology, we demonstrate its use on a case study. The selected case study is the system-level design of an active knee prosthesis driven by an MACCEPA actuator, under the presence of a periodic/real-life dynamical task that is defined in Section 2.4. Note that the proposed design selection methodology is generic enough to be applicable to any VSA platform—in addition to the selected case study—through appropriate modifications in its dynamic and optimization model. This section presents details related to the constituents of the developed design selection methodology as they apply to the case study.

https://doi.org/10.1017/S0263574718001248 Published online by Cambridge University Press

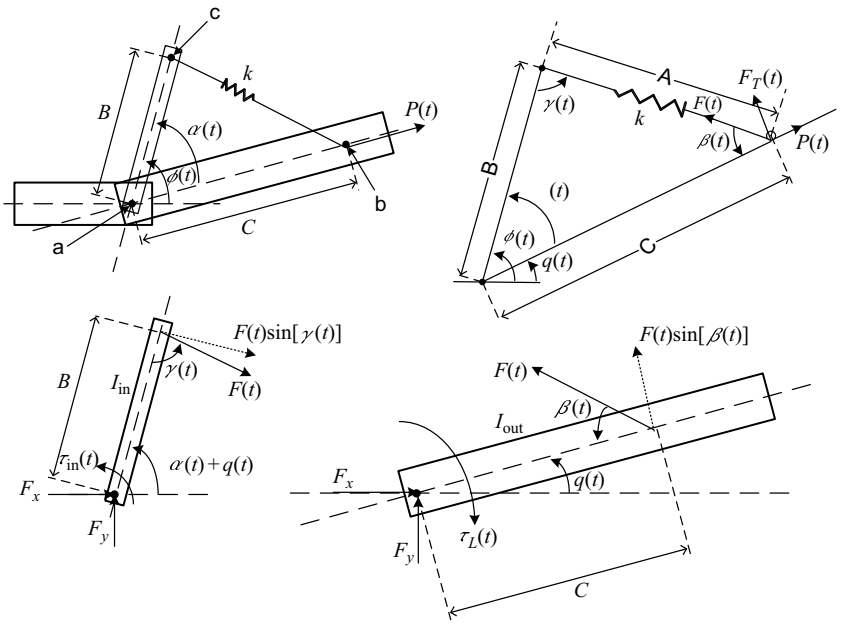

Fig. 3. MACCEPA kinematics and free-body diagram.

3.1. Common compliant actuation principle

For ensuring a systematic comparative methodology based on a common underlying actuation principle, MACCEPA has been preferred as the compliant actuator of choice with its simple mechanical structure and principle of operation, for the single-DoF robotic prosthesis design.

Figure 3 provides a schematic representation and the free-body diagram of a single-DoF MACCEPA-powered robotic prosthesis along with variables/parameters required to define its kinematics/dynamics.

MACCEPA actuator consists of a rotational motor situated at point "a" responsible for controlling the joint equilibrium position $\phi(t)$, along with a linear motor for regulation of joint compliance by controlling the spring pretension $P(t)$. Friction and other nonlinear effects such as joint clearance, backlash, so on, have been neglected in modeling of the selected compliant actuator for the case study. Note that neglecting these effects does not limit the validity of the presented comparative design methodology and its corresponding results. Dynamical equations of the system can be obtained, based on the free-body diagram, as follows:

$$\tau_{\text{in}}(t) = \quad I_{\text{in}}\,\ddot{\phi}(t) \;+\; k\;B\;C\;S\;\sin\left(\phi(t) - q(t)\right) \tag{2}$$

$$\tau_{\text{L}}(t) = -I_{\text{out}}\,\ddot{q}(t) \;+\; k\;B\;C\;S\;\sin\left(\phi(t) - q(t)\right) \tag{3}$$

where

$$S = 1 + \frac{P(t) - (C - B)}{\sqrt{B^2 + C^2 - 2\;B\;C\;\cos\left(\phi(t) - q(t)\right)}} \tag{4}$$

and $\tau_{\text{L}}(t)$ is the externally applied task-specified load torque which acts on the output link. Table I provides a complete list of definitions of parameters used in the system.

We would like to note at this point that any VC actuator can also be designed as an FC or as an STF actuator through imposing appropriate constraints on its design. For example, MACCEPA, in addition to its intended design as a VSA, can also be designed to be operated as a fixed-stiffness system by restricting its spring displacement, $P(t)$, to be a constant trajectory. Furthermore, it can also be designed to operate as an STF actuator where its joint stiffness given by the relation

$$K(t) = k\;B\;C\;S\;\cos\left(\phi(t) - q(t)\right) - k\;B^2\;C^2\;M\;\sin\left(\phi(t) - q(t)\right)^2 \tag{5}$$

https://doi.org/10.1017/S0263574718001248 Published online by Cambridge University Press

Table I. Parameters used to define MACCEPA-powered prosthesis.

Parameter	Description
B	Lever arm (input link) length
C	Distance between the joint and the spring attachment
k	Linear Spring constant
I_{out}	Output link inertia
I_{in}	Input link inertia
$q(t)$	Output link instantaneous position (task trajectory)
$\phi(t)$	Output link equilibrium position
$\tau_{\text{in}}(t)$	Rotational motor input torque
$\tau_{\text{L}}(t)$	Task-specific load torque
$P(t)$	Spring extension due to pretensioning
$F(t)$	Force across linear spring

where

$$M = \frac{P(t) - (C - B)}{\left(B^2 + C^2 - 2\,B\,C\,\cos\left(\phi(t) - q(t)\right)\right)^{\frac{3}{2}}} \tag{6}$$

is made to attain a significantly large value. As a consequence, by imposing proper constraints, system designs with different levels of VC or FC can be generated.

3.2. System-optimal design of the MACCEPA-powered prosthesis

We now present a mathematical formalization of the system-level design optimization problem for MACCEPA-powered prosthesis using the SIM strategy. An important element to consider when designing mobile robots, such as prosthetics, is minimization of physical system weight. In the light of this, we have selected to be our design objective the minimization of peak-to-peak difference of torques supplied through two motors in the system. The system is at the same time required to carry out the dynamical task described by system equations (2) and (3) in addition to meeting the task-specified required motion and load torque trajectories, $q(t)$ and $\tau_L(t)$, respectively. The reason for trying to reduce the necessary motor dynamic torque limits is the fact that physical weight of a motor decreases significantly as the required dynamic torque range decreases. This translates into substantial weight savings in a robotic system driven by compliant actuators, especially when one considers designing multiple-DoF systems of such type. Note also that one may consider using other design objectives that would contribute to aspects, such as kinematics/dynamics, motion ranges, and power consumption. However, in this work the authors have selected as their objective the required dynamic torque range in an attempt to reduce physical system weight.

Motivated by this argument, we formally define the design objective for system-level optimization of the MACCEPA-powered prosthesis as

$$J = \rho_1 J_1 + \rho_2 J_2 \tag{7}$$

Here, J_1 and J_2 are the costs that are responsible for penalization of each motor on the VSA system and are given by

$$J_1 = (\max[u_1(t)] - \min[u_1(t)])^2 \tag{8}$$

$$J_2 = (\max[u_2(t)] - \min[u_2(t)])^2 \tag{9}$$

Also, ρ_1 and ρ_2 are the respective penalization weights for the costs related to each motor as given by

$$u_1(t) = \tau_{\text{in}}(t) \quad \text{and} \quad u_2(t) = \alpha_{\text{scl}} k P(t) \tag{10}$$

Here, α_{scl} is a scaling factor as described below in further detail, and $kP(t)$ is part of the force across the linear spring in the MACCEPA as given by

$$F(t) = k\left(\sqrt{B^2 + C^2 - 2BC\cos\left(\phi(t) - q(t)\right)} - (C - B) + P(t)\right) \tag{11}$$

https://doi.org/10.1017/S0263574718001248 Published online by Cambridge University Press

$F(t)$ is the supplied force by the linear motor of MACCEPA and is responsible for regulating the stiffness by varying spring displacement $P(t)$. The cost function J has been constructed in the form of a weighted sum of two objectives J_1 and J_2. While J_1 is responsible to penalize the dynamic torque range of the motor responsible for positioning, J_2 penalizes the dynamic force range of the motor in charge of compliance regulation.

Please also note that the methodology presented in this paper is general enough to be applicable to any kind of variable stiffness actuation structure, including the MACCEPA type, serial type, and antagonistic type. In many VSA structures, including MACCEPA and antagonistic types, the actuation is not decoupled for motion and stiffness change; both motion and stiffness change are achieved by the coupled action of both actuators. Even for certain classes of VSA systems (e.g., series types), where the actuators used for motion and stiffness change may be decoupled, this is commonly valid in ideal quasi-static conditions where the system is not undergoing a dynamical scenario. Many real-life applications, including the ones considered in this paper, such as walking and running, are highly dynamic tasks where the input torques are coupled through the dynamics of the system, as well as friction effects under external loading. Along these lines, the presented methodology is general and can be applied to all VSA types, including most series types. Whenever the coupling is weak, the Pareto-front curve will capture this aspect and the coefficients of J_1 and J_2 can be decided accordingly during the design selection process. Also note that these two costs, normally, do not have homogeneous units meaning that while the first one is a torque value, the latter is a force quantity. In order to make sure that the optimization problem is well scaled—in the sense of similarly penalizing each motor's limit—a scaling factor α_{scl}, which is also known in literature as a *characteristic length*, has been used. This scaling factor is used to ensure homogeneity of units as well as an equal scale for each objective term, by multiplying the force value of the second motor to convert it into a virtual torque value, in constructing J_2. This way, both cost components are designed to penalize a torque entity. Finally, ρ_1 and ρ_2 are used as weights to penalize the torque range on each motor and can be arbitrarily selected for the application of interest. Through varying the values of these weights, one may consider generating a Pareto-set of robot designs each utilizing different motor sizes. This is precisely how the system-optimal robot designs actuated by different levels of VC are generated in scope of the presented design selection methodology.

The aim of the two-phase procedure is to generate a Pareto-set of comparable system-optimal designs for each phase. Each Pareto-front provides all possible system-optimal designs having different combinations of objective weights corresponding to different design preferences. This way, engineers may be able to perform well-informed selections when setting objective weights a priori is not trivial. Note that for a specific preference (i.e., an objective weight combination), finding an optimal solution corresponds to one point on our Pareto-front and is, therefore, a specific case of the proposed method's more generic solution.

Mathematical formalization of the SIM co-design problem—which is used throughout designs carried out in this work for the selected case study—for system-optimal design of MACCEPA-powered knee prosthesis can now be described as follows:

$$\min_{B,\,C,\,k,\,u_1(t),\,u_2(t)} \quad J = \rho_1 J_1 + \rho_2 J_2, \quad \text{subject to} \tag{12}$$

$$\begin{aligned}
0.015 \;&\leq\; B \leq 0.10 \\
0.20 \;&\leq\; C \leq 0.30 \\
15{,}000 \;&\leq\; k \leq 60{,}000 \\
\tau_{\text{in}}(t) = \;& I_{\text{in}}\,\ddot{\phi}(t) \;+\; k\,B\,C\,S\,\sin\left(\phi(t) - q(t)\right) \\
\tau_{\text{L}}(t) = -& I_{\text{out}}\,\ddot{q}(t) \;+\; k\,B\,C\,S\,\sin\left(\phi(t) - q(t)\right) \\
&(u_1(t) \quad u_2(t)) \in \Omega
\end{aligned}$$

Note that optimization takes place, simultaneously, over the complete set of mechanical design variables that are static, in addition to the dynamic control design variables which are infinite dimensional, along with respective static and dynamic constraints. Here, Ω represents the set of admissible

https://doi.org/10.1017/S0263574718001248 Published online by Cambridge University Press

Table II. Simultaneous co-design problem parameter definitions.

Parameter	Definition	Description	Units
d_{m}	$[B\ C\ k]$	Mechanical Design Vector	[m m N/m]
$d_{\mathrm{c}} = [u_1(t)\ u_2(t)]$	$[\tau_{\mathrm{in}}(t)\ \alpha_{\mathrm{scl}} k P(t)]$	Control Design Vector	[Nm Nm]
$[x_1(t)\ x_2(t)]$	$[\phi(t)\ \dot{\phi}(t)]$	State Vector	[rad rad/s]
lb_{m}	[0.015 0.2 15,000]	Lower Bounds on d_{m}	[m m N/m]
ub_{m}	[0.1 0.3 60,000]	Upper Bounds on d_{m}	[m m N/m]

control trajectories which are limited by torque ratings of the motors used in the system, while all the remaining parameters are defined in Table II.

The amount of torque injected from the motors depends, among other factors, on how the storage of potential energy in the springs of the compliant actuator gets regulated during a single gait cycle of the VSA-powered prosthesis. In this regard, an optimally regulated storage of this potential energy will result in an optimal system and is affected by both the optimally selected spring coefficient value, along with optimal link lengths and inertias, and the optimally selected torque trajectories of the motors. Optimal selection of these design variables requires co-optimization of both the static variables of the mechanism/plant (via static optimization) and the dynamic variables of the controller (via optimal control) and leads to system-optimal designs.[20]

In addition, optimization bounds for the mechanical design variables $0.015 \leq B \leq 0.10$ m and $0.2 \leq C \leq 0.3$ m are selected to be within physically allowable values that our designs can accommodate. For the linear spring constant which we bounded as $15{,}000 \leq k \leq 60{,}000$ N/m, we have used the value 33,350 N/m given in MACCEPA datasheet provided by VIACTORS project, as a reference point.[25] We finally need to indicate that parameter values for input and output link inertias, $I_{\mathrm{in}} = 0.1461 B^3$ kg m^2 and $I_{\mathrm{out}} = 0.063$ kg m^2, have been used throughout all optimization runs.

3.3. System-optimal prosthesis designs: Phase-I

Having provided the necessary definitions for system-optimal design of the MACCEPA-powered prosthesis, we may now present the first phase of the proposed design selection methodology. Phase-I generates system-optimal designs with different degrees of VC. Recall that we mentioned in Section 3.2, ρ_1 and ρ_2 as optimization weights that respectively penalize torque rating of each motor on the MACCEPA system, or any VC actuator in general. But also note that, in addition to its mentioned use ρ_2, which penalizes the motor responsible for stiffness variation by regulating spring displacement $P(t)$, can also be utilized as a means of penalizing the amount of compliance variation in the system. A relatively smaller value of ρ_2, compared to ρ_1, corresponds to an actuation system whose compliance is allowed to vary more than a system with a relatively larger value of ρ_2. Using this argument, through continuously increasing the value of ρ_2, it is possible to generate a variety of system-optimal designs ranging from a VC to an FC design. This is precisely how the first phase of homotopy is generated. This process is demonstrated, as it is implemented in this work, on a flow diagram shown in Fig. 4.

In Fig. 4, note the existence of an initialization routine at the start of the process. This first step is implemented in order to make sure that the design optimization procedure is initialized from a feasible design candidate. It works as follows: first, mechanical design variables within physically allowable bounds are selected which consequently establishes a fixed mechanical design. Then, a control optimization problem is carried out on this fixed mechanical design to come up with a system design which is not only feasible but also control optimal. Following the initialization routine, the homotopy process begins with the first simultaneous co-design problem initialized from the initial design and solved for the case $\rho_2 = \rho_2 = 1$. This results in a system-optimal design which actually corresponds to the VC MACCEPA design concept shown at the top of Fig. 1. After that, the process is iteratively advanced further, generating designs, while the value of ρ_2 is continuously increased at each iteration until the system becomes an FC design.

Phase-I acts as the necessary means of transforming designs from VC actuation to FC actuation stage. In addition, Phase-I is used to carry out a very important task by serving as a design mechanism

https://doi.org/10.1017/S0263574718001248 Published online by Cambridge University Press

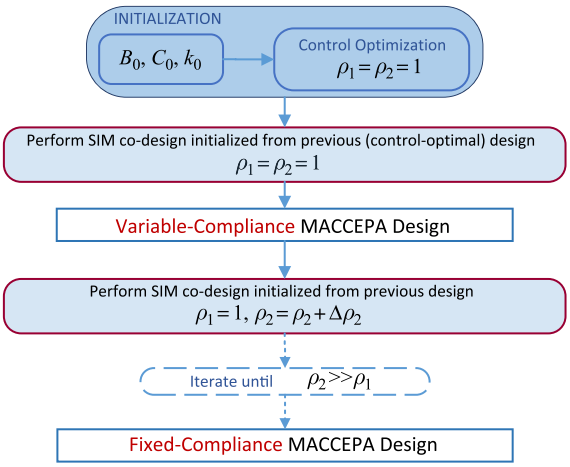

Fig. 4. Homotopy Phase-I.

that generates a Pareto-set of system-optimal robot designs powered by VC actuators. Note that Fig. 4 describes implementation of the homotopic method starting from the case $\rho_1 = \rho_2 = 1$ that ends with $\rho_1 \ll \rho_2$. If a similar process is performed in an opposite direction, starting with a design at $\rho_1 = \rho_2 = 1$ and moving toward a design with $\rho_1 \gg \rho_2$, a complete homotopy of system-optimal designs corresponding to a complete Pareto-set of system designs can be generated. Such a Pareto-set can then be used in the selection of system-optimal robot designs driven by compliant actuators. Within the scope of the developed methodology, such a set of Pareto-optimal designs has been generated using the presented case study.

3.4. System-optimal prosthesis designs: Phase-II

Note that toward the end of Phase-I, the relative value of ρ_2 is made very high in order to enforce a design with FC where variation of $P(t)$ is heavily penalized. This makes $P(t)$ to turn into a constant trajectory. Consequently, during the second homotopy phase which progresses from an FC design toward an STF design, $P(t)$, similarly to the mechanical design variables which are static, can also be treated as a static design variable instead of a dynamic control design variable. As a direct consequence of $P(t)$ becoming a constant trajectory, its effect on the cost function J becomes insignificant and therefore can be taken out of the objective during the second design phase.

After the mentioned modifications take effect, the SIM co-design problem for the MACCEPA-powered prosthesis at design Phase-II can be re-formulated as follows:

$$\min_{B,\,C,\,k,\,P,\,u_1(t)} \quad J = J_1, \quad \text{subject to} \tag{13}$$

$$0.015 \le B \le 0.10$$

$$0.20 \le C \le 0.30$$

$$15{,}000 \le k \le 60{,}000$$

$$-0.1 \le P \le 0.1$$

$$\tau_{\text{in}}(t) = I_{\text{in}}\,\ddot{\phi}(t) + k\,B\,C\,S\,\sin\left(\phi(t) - q(t)\right)$$

$$\tau_{\text{L}}(t) = -I_{\text{out}}\,\ddot{q}(t) + k\,B\,C\,S\,\sin\left(\phi(t) - q(t)\right)$$

$$(u_1(t)) \in \Omega$$

It may be noted here that $u_1(t)$ is now the only control design variable that is dynamic, while $P(t)$, which is from now on denoted by P, is regarded as another static mechanical design variable.

As pointed out earlier, in this design phase which begins with an FC design, homotopy is generated by gradually increasing system's joint compliance, $K(t)$, given in Eq. (5). This idea is actualized by adding an extra dynamical constraint into the co-design problem. The constraint is placed as a

https://doi.org/10.1017/S0263574718001248 Published online by Cambridge University Press

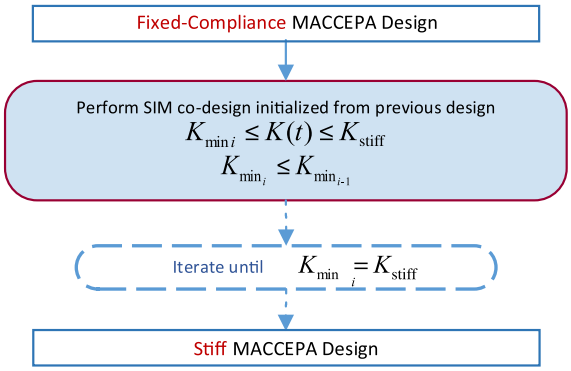

Fig. 5. Homotopy Phase-II.

lower bound, $K_{\min}$, on the value of $K(t)$ and is gradually increased at each design iteration until it approaches to an upper bound, K_{stiff}, which corresponds to a system design having a very large joint stiffness value. This process is illustrated in Fig. 5.

Please note, once again, that the proposed methodology is generic and one can apply the same methodology on multiple VSA types and/or on other task requirements and perform a comparative analysis and come up with a more general design selection methodology. Establishment of such a generic design methodology has significantly greater breadth and is definitely beyond the scope of the presented work. Such an extension will be part of our future research.

4. Implementation Details and Results

Throughout this work, all of the co-design optimization runs for system-optimal design of MACCEPA-powered prosthesis have been conducted using the introduced simultaneous strategy, which is a hybrid optimization method. Being a coupled dynamic optimization problem, it is solved numerically using the "Propt" module by Tomlab. Tomlab is a Matlab-based general purpose optimization environment, and its Propt module employs pseudospectral collocation methods for solving dynamic optimization problems. In defining our dynamical optimization problems, we have used a Fourier pseudospectral method option supplied with Propt which uses in its basis trigonometric functions to represent dynamical states and controls. This selection was due to the fact that our task trajectories are periodic, which suggests that our control and state trajectories are also expected to be periodic. We have used the "Snopt" solver of Propt using 50 collocation points sampled over a single period of design trajectories in obtaining the presented dynamical optimization results, while all other settings are left at their default values. Snopt is a large-scale nonlinear programming (NLP) solver that is sequential quadratic programming based and was developed by the Stanford Systems Optimization Laboratory (SOL).[26]

Please also note that solution of the presented methodology is based on local optimizers. Global search methods for dynamic optimization (in our case optimal control) problems are still in their infancy and therefore are not well established yet as tools to be integrated in the design problems presented in this work. However, please note that our methodology does not exclude use of global optimizers, once they become available. Throughout our implementations, a value of $\alpha_{\text{scl}} = 0.065$ has been selected to be used as a characteristic length which we introduced in Section 3.2. Finally, we would like to add that all of the optimization runs carried out in this work have been implemented using a single core of an 8-core 3.20 GHz Intel Xeon X5482 PC having 8 GB RAM. Each co-design run using the presented SIM strategy took, on average, around 0.5 s to converge to the system-optimal design.

Local optimality of a co-design problem is guaranteed[19] when necessary conditions for optimality of both the mechanical and the control optimization problems are satisfied. These necessary conditions happen to be the Karush Kuhn Tucker conditions for the mechanical design optimization and the Pontryagin's maximum principle for the optimal control problem, respectively. The state-of-the-art solvers within Tomlab implemented throughout optimization runs in the presented work guarantee satisfaction of both conditions.[26,27] Propt utilizes a pseudospectral method whose convergence has been shown to be mathematically equivalent to satisfaction of Pontryagin's maximum

https://doi.org/10.1017/S0263574718001248 Published online by Cambridge University Press

Table III. Co-design optimization results ($\rho_1 = \rho_2 = 1$).

Mechanical design		Motor torque limits		
Initial	**Optimal**	**Initial [Nm]**	**Optimal [Nm]**	**Reduction [%]**
$J_0 = 3159.84$	$J^* = 801.29$	$\Delta u_1 = 22.2827$	$\Delta u_1^* = 20.0742$	9.91
$B_0 = 0.045$ m	$B^* = 0.0844$ m	$\Delta u_2 = 51.6074$	$\Delta u_2^* = 19.9561$	61.33
$C_0 = 0.235$ m	$C^* = 0.300$ m			
$k_0 = 33{,}000$ N/m	$k^* = 15{,}000$ N/m			

principle. In particular, when the solver indicates that an optimal solution was found, the solution satisfies necessary conditions of optimality and it is guaranteed that this solution cannot be improved by an infinitesimal change in the trajectory. Therefore, it can be theoretically concluded that system-level local optimality of the obtained design solutions are guaranteed up to a precision.

Before moving on to presenting homotopies that resulted from the two design phases, we would like to provide the obtained co-design results for the case $\rho_1 = \rho_2 = 1$. This case corresponds to a system-optimal design where the dynamic torque ranges of the two motors are equally penalized. Table III includes values of the optimal mechanical design variables that belong to the system-optimal design achieved by the presented SIM co-design approach. The table also provides values for each motor's dynamic torque range Δu_1 and Δu_2. These values are the differences between maximum and minimum values of torque trajectories and determine the amounts of dynamic torques that need to be generated by each motor that is employed in the system. It can be viewed that reductions in required torques of around 10% and 60% have been achieved through co-design for the motors responsible for positioning and compliance regulation, respectively.

Note also that solution of any optimal control problem, hence a co-design problem, depends on the selected dynamical task for a given application. This dynamical task for our problem happens to be the nominal motion and load torque trajectories which were defined in Section 2.4. In the meantime, continuity of solutions shall ensure that small changes in nominal task trajectories would also lead to small changes in the resulting solution trajectories. In this regard, a numerical sensitivity analysis to demonstrate continuity of solutions for perturbations in task trajectories had been performed in ref. [20]. In particular, optimization runs using task trajectories whose magnitudes and speeds were perturbed from their nominal values by certain percentages have been carried out. The resulting solution trajectories were then compared to the nominal ones. The results have shown that percentage deviations from nominal optimal solutions increase gradually as expected, but always stay under 10% even when 20% perturbations on both task motion and torque trajectories were applied. These observations had helped validate the continuity of the optimal solution trajectories obtained by the proposed co-design approach. We have also verified validity of our solutions through dynamical simulations, where the optimal solutions have been used to control the MACEPPA actuator along the desired trajectory under the specified load torque.

In the following subsections, results for the related homotopies are presented in two parts corresponding to design Phases-I and II as discussed previously.

4.1. Phase-I results: VC to FC

Implementation of the homotopic approach at Phase-I for system-optimal design of the MACCEPA-powered prosthesis has resulted in the Pareto-set designs which are illustrated by the Pareto-front that is shown in Fig. 6.

In particular, the Pareto-front represents a number of system-optimal prosthesis designs that range from the case with $\rho_1 = 1$, $\rho_2 \to 0$. This practically corresponds to a system-optimal design that uses only the motor responsible for compliance variation in carrying out the dynamical task, toward another design with $\rho_1 = 1$, $\rho_2 \to \infty$. The latter corresponds to another system-optimal design only utilizing its motor in charge of positioning and hence is a design with FC. Every other system in between these two cases corresponds to designs with different degrees of VC. Note that the Pareto-optimal designs in the figure have been classified into three regions with corresponding labels. Pareto-points in Region-I correspond to system-optimal designs which are biased more toward a VC

https://doi.org/10.1017/S0263574718001248 Published online by Cambridge University Press

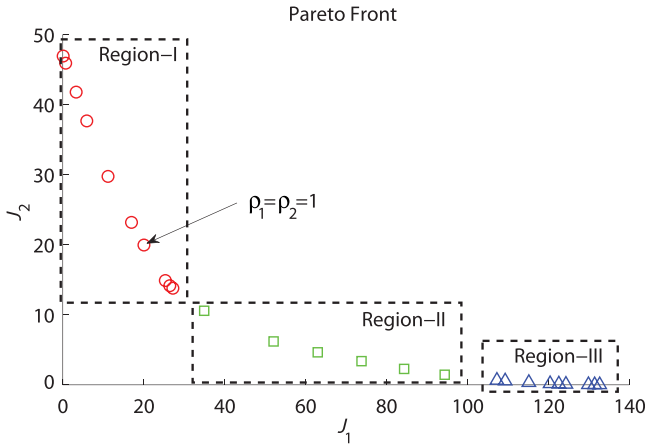

Fig. 6. Pareto-optimal designs.

design where, in most cases, the motor responsible for compliance variation is relatively less penalized. Penalization weights in this region range from $\rho_1 = 1$, $\rho_2 \to 0$ to $\rho_1 = 1$, $\rho_2 = 4$. Beginning with Region-II of the Pareto-optimal designs, where penalization weights range between $\rho_1 = 1$, $\rho_2 = 10$ to $\rho_1 = 1$, $\rho_2 = 1000$, the systems start to get biased more toward an FC state due to increasing value of ρ_2. An increased value of ρ_2 imposes a higher penalty on the usage of the compliance motor. Designs starting with $\rho_1 = 1$, $\rho_2 = 3000$ and continuing until $\rho_1 = 1$, $\rho_2 \to \infty$ belong to Region-III of the Pareto-front. This region is dictated by a heavy penalization on the compliance motor, and therefore the designs in this region can be considered as FC systems for all practical purposes. Table IV illustrates a homotopy of optimal control design trajectories which belong to system-optimal prosthesis designs from all three regions of the Pareto-front.

Once the system designs reach the FC state, the homotopy is carried further using the reformulated co-design problem presented in Section 3.4.

4.2. Phase-II results: FC to rigid systems

In this phase of the homotopic process, $u_2(t)$ is no longer a dynamic trajectory but gets designed as a static design variable along with the other mechanical design variables as mentioned earlier. This makes $u_1(t)$ the only dynamic trajectory for system designs having FC. Table V illustrates a number of optimal trajectories for $u_1^*(t)$ and $u_2^*(t)$ that belong to system-optimal designs corresponding to the Phase-II of the homotopic process.

As it can be observed, peak-to-peak difference values of the torque trajectories for $u_1^*(t)$ increase as the designs evolve from FC toward the design powered by STF actuation. Here, an increasing value on the minimum value of joint stiffness, $K_{\min}$, has been placed as a lower constraint on system's joint stiffness $K(t)$ in order to enforce a system-optimal design that is driven by STF actuation. In the meantime, $u_2^*(t)$, which is now a constant trajectory can be monitored to decrease its value in negative direction. In the following section, a detailed discussion related to the presented results is provided.

5. Discussion

In this section, we will first discuss the advantages of the presented design selection methodology. After that, essential benefits that are obtained due to the implementation of a system-level co-design approach will be discussed in detail.

Results related to the presented comparison methodology were demonstrated in Section 4, which were categorized under two main design homotopy phases corresponding to VC and FC regimes, respectively. Primary significance of generating system-optimal designs in these homotopy phases with different degrees of VC and/or FC is to facilitate a well-informed decision-making strategy for engineers in regard to their particular applications. In what follows, a thorough discussion on each of these design phases and how they can be utilized for studying design trade-offs and in selecting application-specific system designs are provided.

https://doi.org/10.1017/S0263574718001248 Published online by Cambridge University Press

Table IV. Phase-I homotopy design trajectories.

$u_1^*(t)$ trajectories	$u_2^*(t)$ trajectories
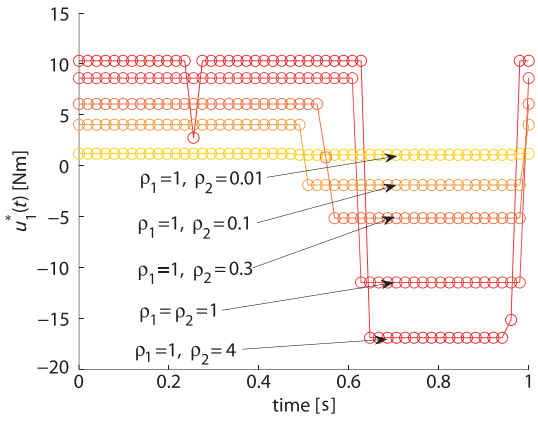	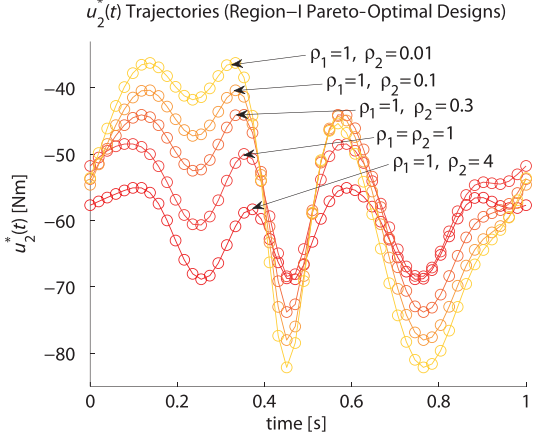
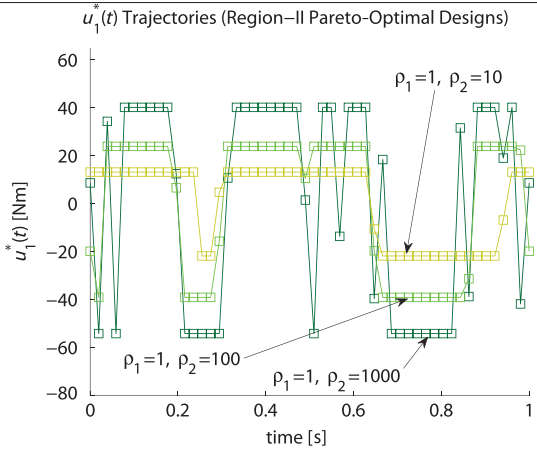	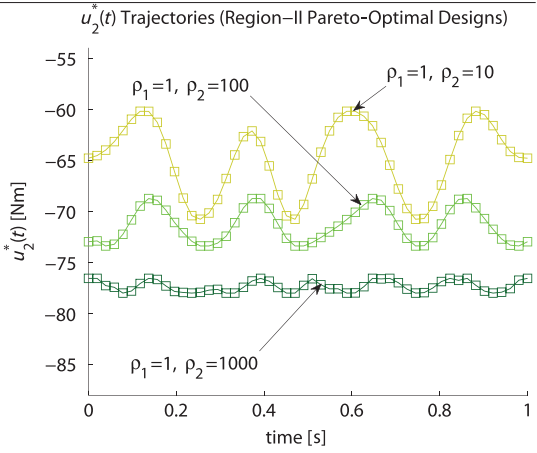
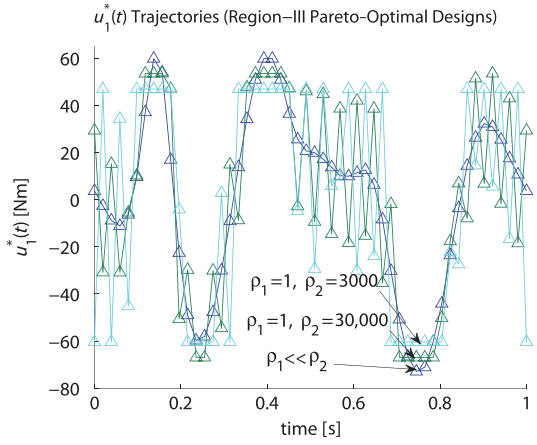	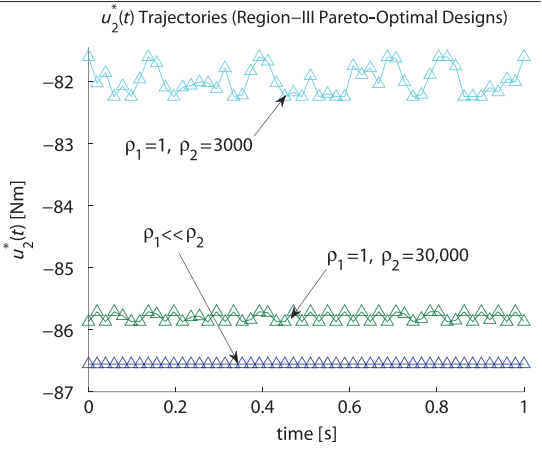

5.1. VC design phase

The first design phase had resulted in a Pareto-set of system-optimal designs that were illustrated in Fig. 6, consisting of prosthesis designs with different degrees of compliance variation. Having such a Pareto-set allows an optimal selection of designs with varying degrees of compliance variation for given applications of interest and provides a systematic decision-making strategy. Such a decision-making process can be better illustrated on the set of Pareto-optimal designs shown in Fig. 7.

The figure highlights three system-optimal designs that may be selected depending on a particular scenario. For instance, if design simplicity is of major concern in an application where a single motor is to be utilized, then Designs #1 and #2 which both employ a single motor may be selected. In such

https://doi.org/10.1017/S0263574718001248 Published online by Cambridge University Press

Table V. Phase-II homotopy design trajectories.

$u_1^*(t)$ trajectories	$u_2^*(t)$ trajectories
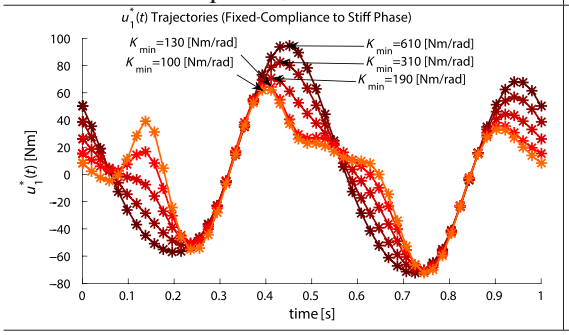	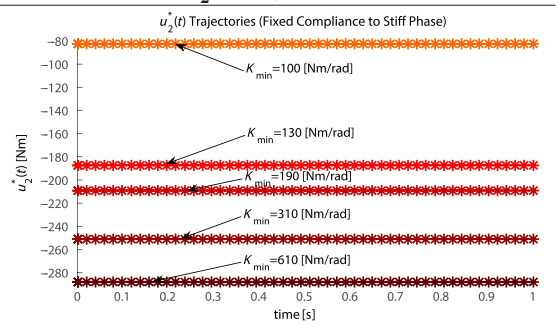

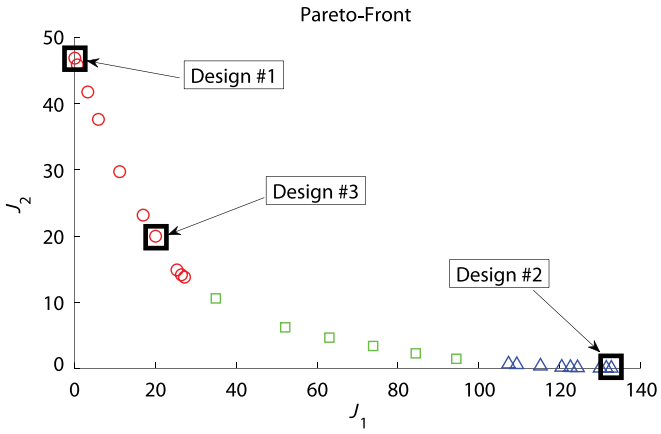

Fig. 7. Selection of Pareto-optimal designs.

a case, Design #1 may be preferred over Design #2 since it requires a rated torque of around 47 Nm, whereas Design #2 requires around 135 Nm of torque. In the meantime, another application may happen to suggest the input link of the MACCEPA to be grounded. In such a scenario a designer would prefer Design #2 where only the positioning motor, which will also be grounded, is employed to carry out the dynamical task. On another scenario where it may be favorable to have the system with the best weight distribution properties and the lowest physical weight, Design #3 where both motors have torque ratings of 20 Nm may be selected. It ultimately boils down to an engineering task to select the particular design from the set of Pareto-optimal systems that are guaranteed to perform at their full potential. Significance of having a set of system-optimal designs is that it empowers such decision-making process.

Table IV provides optimal torque trajectories which belong to a number of selected system-optimal designs from this Pareto-front. Note that these torque trajectories altogether form a continuum of optimal control designs that begin with a completely VC design corresponding to $\rho_1 = 1$, $\rho_2 = 0.01$, and move further into an FC design with $\rho_1 = 1$, $\rho_2 \to \infty$. As this homotopy progresses, dynamic torque range of the motor responsible for compliance variation is observed to start with a maximum value and decrease toward zero, while an exact opposite observation is made for the motor responsible for positioning. In addition to decreasing levels of compliance variation, system designs also become less compliant as the design homotopy evolves further into the FC phase. This may be observed by decreasing levels of torque offset for compliance motor, which starts around -57 Nm at the beginning of Region-I shown in Table IV and decreases in negative direction to around -86.5 Nm at the end of Region-III which practically corresponds to a system design with FC. This observation physically translates into system designs where the amount of compression on linear MACCEPA spring is continually increased, resulting in increased joint stiffness.

The Region-I of the Phase-I homotopy is characterized by a continuum of optimal $u_1^*(t)$ trajectories of bang-bang type that keep increasing in peak-to-peak amplitude. Meanwhile, the optimal

https://doi.org/10.1017/S0263574718001248 Published online by Cambridge University Press

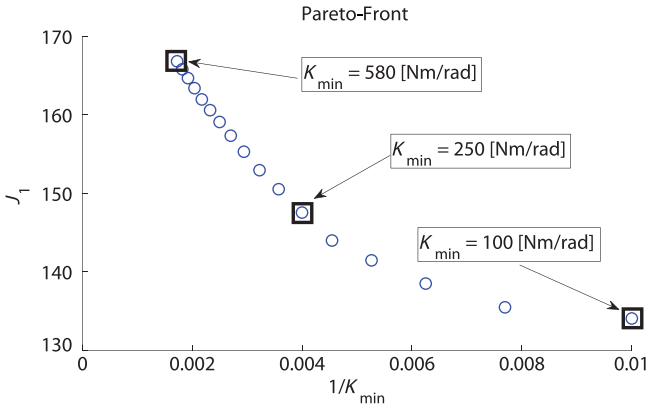

Fig. 8. Pareto-optimal designs with FC.

trajectories for $u_2^*(t)$ keep decreasing their amplitude as system designs start to get biased toward FC. In addition, designs begin to have an increasing joint stiffness as recently discussed.

The Region-II of the Phase-I homotopy presents designs with an interesting nature. As depicted in Table IV, optimal control trajectories for $u_1^*(t)$ corresponding to designs in this region keep increasing in peak-to-peak amplitude while exhibiting a highly oscillatory behavior. At the same time, trajectories for $u_2^*(t)$ keep decreasing in both peak-to-peak amplitude and offset values. Such oscillatory behavior can be explained as follows. This particular region of the homotopic process represents a transient region where the motor responsible for positioning of the output link of the MACCEPA-powered prosthesis additionally has to perform a task of active vibration cancellation that is required to cancel out vibrations caused by excitement of certain modes. These modes are specific to systems in this homotopy region, having specific natural frequencies mainly dictated by their joint compliance.

As the system designs move further into Region-III of the Phase-I homotopy, optimal trajectories for $u_1^*(t)$ continue increasing further in peak-to-peak amplitude until a maximum value corresponding to a system design with FC has been reached. The optimal trajectories for $u_2^*(t)$ on the other hand keep decreasing in peak-to-peak amplitude until they reach zero for the design with fixed stiffness. Also note that the oscillations completely vanish toward the end of this homotopy region. This is due to the fact that natural frequency of the systems keep increasing to a certain point where the system modes are no longer excited. This physically means that the offset torque value for $u_2^*(t)$ is increased further in negative direction, causing further compression on the MACCEPA linear spring, resulting in increased joint stiffness.

5.2. FC design phase

The second main design homotopy phase corresponds to designs having completely FC and is named as Phase-II. It may be observed that, similarly to the VC design regime, the designs in this phase may also be considered to establish a Pareto-set of system-optimal designs, this time with various levels of *FC*. More specifically, a Pareto-curve may be generated between the cost related to the positioning motor, J_1, and the minimum amount of joint compliance, $1/K_{\text{min}}$, in a given design. Such a Pareto-curve, which is given in Fig. 8, represents a set of system-optimal designs where any reduction in the system objective, J_1, necessitates an increase in the minimum value of system joint compliance.

Such a Pareto-curve can be explained by the fact that there exists a trade-off between the required actuation effort and the amount of compliance in a dynamical system with FC undergoing periodic motions. Compared to an STF design, a more compliant system can store more potential energy in its joint and can later reuse this stored energy in reducing its actuation effort. This leads to the use of smaller motors as already mentioned. On the other hand, increasing the joint compliance of a system decreases its bandwidth. Availability of such a Pareto-set enables engineers study such trade-offs and make insightful design decisions on the level of actuation effort and system bandwidth needed for their applications.

Table V illustrates control trajectories that belong to system-optimal prosthesis designs in this phase. As it can be observed, trajectories of $u_1^*(t)$ start from an FC system design having a minimum

https://doi.org/10.1017/S0263574718001248 Published online by Cambridge University Press

joint stiffness value of $K_{\min} = 100$ Nm/rad and keep increasing in peak-to-peak amplitude until the homotopy is advanced to an STF system with a minimum joint stiffness of $K_{\min} = 610$ Nm/rad. In the meantime, optimal trajectories for $u_2^*(t)$ corresponding to the same system designs, which happen to be constant trajectories during this design phase, keep increasing in negative direction. This can be physically interpreted as further compression on the MACCEPA linear spring until the system behaves as an STF design. This terminates the Phase-II part of the homotopic design process.

5.3. Advantages of co-design

Another significant advantage of the presented design methodology is due to the effectiveness of performing co-design. Co-design is the utilized design approach throughout generated solutions, in achieving substantial performance improvements instead of using domain-specific optimization methods, such as optimal control alone. Impressive improvements in regard to physical system weight which leads directly to higher energy efficiency are possible as a result of performing system-level design optimization as opposed to the more conventionally employed domain-specific techniques. Reductions that can be obtained in physical weight of the system can be better appreciated using a motor selection example. The obtained optimal motor torque limits in Table III show that peak-to-peak amplitude of the motor responsible for compliance regulation was reduced from a value of over 50 Nm for the initial system to a value of 20 Nm for the system-optimal design through the implemented co-design strategy. This means that the initial system design, which also happens to be a design whose control subsystem has been optimized via the initialization routine, requires the use of a motor capable of supplying such torque. This torque can be provided by a Maxon RE-50 motor in combination with the gear-head capable of generating the 50 Nm of maximum continuous torque via a reduction of 100 : 1 and comes at the weight of 2600 g. On the contrary, the system-optimal design achieved by the simultaneous strategy requires a torque rating of only 20 Nm. This can be provided by a Maxon RE-40 motor in combination with the gearhead that generates up to 30 Nm of torque via a reduction of 43 : 1 and comes at a weight of only 1280 g.[28] This analysis clearly indicates how significant it is to utilize co-design methods on robots driven by VC actuators and how substantial the attained overall weight reductions can be.

In addition to the improvements obtained in weight reductions, the implemented co-design method delivers significant reductions in apparent inertias of the motor–gearhead combinations. In this regard, the initial design which suggests the use of the Maxon RE-50 motor has an apparent inertia of 0.66 kg m^2 while the system-optimal design with the RE-40 motor has an apparent inertia of only 0.03 kg m^2. Such a substantial reduction in apparent inertia results in a system with higher bandwidth due to the existence of an inverse relationship between a system's reflected inertia and its natural frequency. As a consequence, improvement in system bandwidth is another benefit of the presented co-design method on VC robotic systems.

It is crucial to note here that these design improvements, which are obtained for a single-DoF robotic system, are expected to lead toward substantially more impressive gains especially when multi-DoF applications are considered.

6. Conclusion

This work introduces for the first time an integrated design selection methodology which provides an integrated set of system-optimal designs of robotic systems driven by compliant actuators spanning a range of designs starting from VC to FC and ending with systems powered by STF actuation. A homotopy-based design approach facilitates integrity of the developed methodology by maintaining continuity among generated designs. The developed methodology which is based on Pareto-optimality concepts allows roboticists to select designs from among a variety of system-optimal robots driven by actuators with different degrees of VC or FC, depending on specific design scenarios. It is important to note that the comparative methodology is based on a system-optimal formulation and solution as compliantly actuated robotic systems that get designed using domain-specific conventional approaches result in under-performing systems, in other words designs that are not *system* optimal. In order to exploit the full potential of these systems which offer substantial benefits in applications that require safety, high performance, and energy-efficiency, co-design techniques which propose a *system*-level design approach by accounting design interactions among sub-disciplines are implemented throughout the work.

https://doi.org/10.1017/S0263574718001248 Published online by Cambridge University Press

References

1. G. A. Pratt and M. M. Williamson, "Series Elastic Actuators," *IEEE/RSJ International Conference on Intelligent Robots and Systems* (1995) pp. 399–406.
2. J. W. Sensinger and R. F. Weir, "Design and Analysis of a Non-backdrivable Series Elastic Actuator," *IEEE International Conference on Rehabilitation Robotics* (2005) pp. 390–393.
3. E. C. Martinez-Villalpando, J. Weber, G. Elliot and H. Herr, "Design of an Agonist-Antagonist Active Knee Prosthesis," *IEEE/RAS-EMBS International Conference on Biomedical Robotics and Biomechatronics* (2008) pp. 529–534.
4. K. W. Hollander, R. Ilg, T. Sugar and D. Herring, "An efficient robotic tendon for gait assistance," *J. Biomech. Eng.* **128**(5), 788–791 (2006).
5. O. Tokatli and V. Patoglu, "Series Elastic Actuation for Force Controlled Micro-Manipulation," *IEEE International Conference on Mechatronics (ICM)* (2011) pp. 421–426.
6. H. Schempf, C. Kraeuter and M. Blackwell, "Roboleg: A Robotic Soccer-Ball Kicking Leg," *IEEE International Conference on Robotics and Automation* (1995) pp. 1314–1318.
7. M. Okada, S. Ban and Y. Nakamura, "Skill of Compliance with Controlled Charging/Discharging of Kinetic Energy," *IEEE International Conference on Robotics and Automation* (2002) pp. 2455–2460.
8. D. Paluska and H. Herr, "The effect of series elasticity on actuator power and work output: Implications for robotic and prosthetic joint design," *Rob. Auton. Syst.* **54**(8), 667–673 (2006).
9. S. A. Migliore, E. A. Brown and S. P. DeWeerth, "Biologically Inspired Joint Stiffness Control," *IEEE International Conference on Robotics and Automation* (2005) pp. 4508–4513.
10. A. Bicchi, G. Tonietti and R. Schiavi, "Safe and Fast Actuators for Machines Interacting with Humans," *IEEE Technical Exhibition Based Conference on Robotics and Automation* (2004) pp. 17–18.
11. F. Petit, W. Friedl, H. Hoppner and M. Grebenstein, "Analysis and synthesis of the bidirectional antagonistic variable stiffness mechanism," *IEEE/ASME Trans. Mechatron.* **20**(2), 684–695 (2015).
12. R. V. Ham, B. Vanderborght, M. V. Damme, B. Verrelst and D. Lefeber, "MACCEPA: The Mechanically Adjustable Compliance and Controllable Equilibrium Position Actuator for 'Controlled Passive Walking'," *IEEE International Conference on Robotics and Automation* (2006) pp. 2195–2200.
13. A. Jafari, N. G. Tsagarakis, B. Vanderborght and D. G. Caldwell, "A Novel Actuator with Adjustable Stiffness (AwAS)," *IEEE/RSJ International Conference on Intelligent Robots and Systems* (2010) pp. 4201–4206.
14. M. Yalcin, B. Uzunoglu, E. Altintepe and V. Patoglu, "VnSA: Variable Negative Stiffness Actuation Based on Nonlinear Deflection Characteristics of Buckling Ceams," *IEEE/RSJ International Conference on Intelligent Robots and Systems* (2013) pp. 5418–5424.
15. A. Bicchi and G. Tonietti, "Fast and soft arm tactics: Dealing with the safety-performance tradeoff in robot arms design and control," *IEEE Rob. Autom. Mag.* **11**(2), 22–23 (2004).
16. M. Garabini, A. Passaglia, F. Belo, P. Salaris and A. Bicchi, "Optimality Principles in Variable Stiffness Control: The VSA Hammer," *IEEE/RSJ International Conference on Intelligent Robots and Systems* (2011) pp. 3770–3775.
17. S. Haddadin, F. Huber and A. Albu-Schffer, "Optimal Control for Exploiting the Natural Dynamics of Variable Stiffness Robots," *IEEE International Conference on Robotics and Automation* (2008) pp. 3347–3354.
18. D. L. Peters, P. Y. Papalambros and A. G. Ulsoy, "Relationship between Coupling and the Controllability Grammian in Co-design Problems," *American Control Conference* (2010) pp. 623–628.
19. H. K. Fathy, J. A. Reyer, P. Y. Papalambros and A. G. Ulsoy, "On the Coupling between the Plant and Controller Optimization Problems," *American Control Conference* (2001) pp. 1864–1869.
20. A. Kamadan, G. Kiziltas and V. Patoglu, "Co-design strategies for optimal variable stiffness actuation," *IEEE/ASME Trans. Mechatron.* **22**(6), 2768–2779 (2017).
21. S. W. et al., "Variable Stiffness Actuators: Review on Design and Components," *IEEE/ASME Transactions on Mechatronics*, **21**(5), 2418–2430 (2016).
22. I. Hussain, A. Albalasie, M. I. Awad, L. Seneviratne and D. Gan, "Modeling, control, and numerical simulations of a novel binary-controlled variable stiffness actuator (bcvsa)," *Front. Rob. AI* **5**(68), 1–17 (2018).
23. R. T. Marler and S. Arora, "Survey of multi-objective optimization methods for engineering," *Struct. Multidiscip. Optim.* **26**(6), 369–395 (2004).
24. E. C. Martinez-Villalpando and H. Herr, "Agonist-Antagonist Active Knee Prosthesis: A Preliminary Study in Level-Ground Walking," *J. Rehab. Res. Dev.* **46**(3), 361–374 (2009).
25. VIACTORS, "Maccepa datasheet," June 2017, URL: http://www.viactors.org.
26. P. E. Gill, W. Murray and M. A. Saunders, "SNOPT: An SQP Algorithm for Large-Scale Constrained Programming," *Technical Report* (Stanford University, 1997).
27. R. Fletcher and S. Leyffer, "Nonlinear Programming without a Penalty Function," *Technical Report* (University of Dundee, 1997).
28. Maxon Motor AG, "Maxon motor online shop," June 2017, URL: http://www.maxonmotor.com.

https://doi.org/10.1017/S0263574718001248 Published online by Cambridge University Press